

LASER APPLICATIONS

https://doi.org/10.1070/QEL17223

Laser adaptive holographic hydroacoustic intensimeter

R.V. Romashko, Yu.N. Kulchin, V.P. Dzyuba, D.V. Storozhenko, M.N. Bezruk

Abstract. **A new type of a vector hydrophone, a laser adaptive hydroacoustic intensimeter, is investigated. Two identical, spatially separated coil-type sensors are used as a primary receiver of the acoustic signal. The signals received at the sensor output are phase demodulated in a two-channel adaptive holographic interferometer based on two dynamic holograms multiplexed in a CdTe photorefractive crystal. Using a laser intensimeter, the acoustic field formed in a limited volume is studied. The performance characteristics of the intensimeter are determined experimentally; its threshold sensitivity, according to the acoustic field intensity, constitutes 0.1×10^{-13} W m^{-2}.**

Keywords: *vector-phase hydrophone, fibre-optic sensor, adaptive interferometer, dynamic hologram, photorefractive crystal.*

The solution of such problems as studying the underwater conditions, ocean monitoring, underwater communication, and a number of others is inextricably linked with the development of effective means for recording hydroacoustic signals. Most modern acoustic receivers employ electric converters (piezoelectric, electrodynamic, capacitive, etc.), which have a number of disadvantages that in certain cases make it difficult to use them for recording ultra-weak acoustic signals [1, 2]. In this regard, optical and, above all, fibre-optic receivers of acoustic signals have gained significant development [3, 4]. At the same time, the use of interferometric principles in designing the acoustic receivers opens up prospects for detecting ultra-weak signals [5].

Interferometric systems, due to their high sensitivity, are significantly affected by external noise factors (random mechanical effects, temperature, pressure drift, etc.), which in practice in most cases nullifies all the advantages of such systems. The use of electronic stabilisation systems in the interferometer [6, 7] leads to a significant complication of the measuring system, making it difficult or even impossible to build multichannel interferometric schemes, since it is necessary to implement a stabilisation scheme in each channel. As was shown in work [8], the use of dynamic holograms formed in photorefractive crystals (PRC) in interferometers is one of the most effective solutions for stabilising the interferometer's operating point. In papers [9–12], approaches for recording weak acoustic and hydroacoustic signals using adaptive holographic interferometers are proposed.

At the same time, there are problems in which, in addition to recording an acoustic signal, it is also necessary to carry out bearing of its sources. Such problems can be solved using a vector-phase approach, the essence of which is to record, along with the acoustic pressure amplitude, also the vibrational velocity phase of the medium particles (or the acoustic pressure gradient in the wave) [13, 14]. To implement the vector-phase approach, it is necessary to provide simultaneous measurement of the acoustic signal at three pairs of points spaced apart in three orthogonal directions on some spatial base, which entails the need of using multi-channel measuring systems. At the same time, the few types of vector-phase hydroacoustic receivers available today, like most point hydrophones, are designed on an electrical element base [13, 15]. This leads to the existence of problems in such receivers, which are characteristic of electric hydrophones (electromagnetic interference, the presence of aggressive media, etc.), which are repeatedly complicated in a vector-phase receiver due to the need to provide multi-channel measurement. In works [16, 17], the possibility of recording signals using an adaptive holographic interferometer simultaneously on 6 and 32 channels, respectively, was demonstrated.

In this work, a new type of vector-phase acoustic receiver is proposed and studied, i.e. a laser adaptive hydroacoustic intensimeter based on a two-channel adaptive holographic interferometer and fibre-optic sensors, which allows recording the projection of vector acoustic characteristics, such as pressure gradient, vibrational velocity, and vibrational acceleration.

The flux density vector $\boldsymbol{I}(\omega)$ of acoustic energy (acoustic intensity vector) is defined in frequency domain as a real part of the product of complex pressure $p(\omega)$ and vibrational velocity $\boldsymbol{V}(\omega)$ [18]:

$$\boldsymbol{I}(\omega) = 0.5\mathrm{Re}[p(\omega)\boldsymbol{V}^{*}(\omega)], \tag{1}$$

where the vibrational velocity is determined by the pressure gradient ∇p and medium density ρ:

$$\boldsymbol{V}(\omega, r) = -\frac{\nabla p(\omega)}{\mathrm{i}\rho\omega}, \tag{2}$$

$$\nabla p(\omega) = \frac{p_1(\omega) - p_2(\omega)}{\delta x}, \tag{3}$$

where $p_1(\omega)$ and $p_2(\omega)$ are the complex pressure at two points in space located at a distance δx. Thus, two sensing elements located at a distance $l = \delta x$ ensure a projection of the intensity

R.V. Romashko, Yu.N. Kulchin, V.P. Dzyuba, D.V. Storozhenko, M.N. Bezruk Institute of Automation and Control Processes, Far Eastern Branch, Russian Academy of Sciences, ul. Radio 5, 690041 Vladivostok, Russia; e-mail: romashko@iacp.dvo.ru

Received 13 December 2019; revision received 30 January 2020
Kvantovaya Elektronika **50** (5) 514–518 (2020)
Translated by M.A. Monastyrskiy

vector $I_x(\omega)$ on the direction x provided the acoustic pressure spectrum $p(\omega)$ is synchronously measured at these two points.

The scheme of a laser adaptive holographic hydroacoustic intensimeter is shown in Fig. 1. The sensor element of the intensimeter is two identical fibre-optic sensors located at distance $\lambda_{ac}/10$ from each other (λ_{ac} is the smallest wavelength of the acoustic field). Each sensor is made in the form of a foamed-polystyrene cylinder with a diameter of 3 cm and a length of 4 cm, on which a multimode fibre (core diameter 62.5 μm, numerical aperture NA = 0.22) with a length of 3 m (30 turns) is wound.

The optical part of the laser intensimeter is implemented as follows. The Nd:YAG laser radiation (λ = 1064 nm, output power 1 W) passes through the half-wave plate and polarising beam splitter, being divided into signal and reference light waves in a ratio of 1:5 in intensity. The reference wave, elliptically polarised after passing through the quarter-wave plate, is directed to the CdTe photorefractive crystal along the crystallographic axis [100]. The crystal sizes are 5 × 5 × 5 mm. The signal wave radiation is repeatedly divided by means of a 1 × 2 fibre-optic splitter into two light waves of the same power, directed to two identical fibre-optical sensors as part of the sensor element of the intensimeter. Mechanical vibrations of the base material of fibre-optic sensors, caused by the action of acoustic pressure, lead to phase modulation of radiation passing through the optical fibre wound on the base.

Signal wave radiation, after passing through fibre-optic sensors, is directed by optical fibres to the PRC along its crystallographic axis [001] in the direction orthogonal to the reference wave. Pairwise interference in the PRC of each of the signal and common reference waves due to the photorefractive effect leads to the recording of two dynamic holograms in the crystal. Vector interaction of an elliptically polarised reference wave with depolarised (after passing through multimode optic fibres) signal waves in such an orthogonal geometry in the cubic-symmetric PRC ensures the fulfilment of quadrature conditions of the adaptive interferometer, which results in its high sensitivity [19, 20]. The intensity of signal waves, being proportional to the acoustic pressure at the location of the sensors, is recorded using photodetectors, whose signals are transmitted to the computer for processing via a two-channel ADC.

It should be noted that the intensimeter sensitivity is determined by the sensitivity of fibre-optic sensors and a two-channel adaptive interferometer. To ensure the reliability of the results obtained with a laser intensimeter, it is necessary that both the paired sensors and the corresponding demodulation channels of the interferometer have the same sensitivity. In this case, the original sensitivity of fibre-optic sensors may vary, even if they are nominally identical (shape, size, amount of wound optical fibre). The sensitivity in different channels of the adaptive interferometer can also be different due to a number of other reasons, such as the heterogeneity of the photorefractive crystal properties in its volume (the light beam of each signal wave hits a certain place in the PRC), the nonuniformity of the division ratio of the fibre-optic splitter, as well as the possible differences in the characteristics of photodetectors. In this regard, in the present work, we used the channel sensitivity calibration of the intensimeter developed [21]. This method consists in introducing a given phase modulation (calibration signal) with variable amplitude into the interferometer channels, constructing a transition characteristic and determining, on its basis, a calibration coefficient for each channel.

Experimental studies of the developed intensimeter were conducted in a test pool with dimensions of 2.93 × 1.72 × 0.6 m, filled with 80% water. The pool was located on a 0.1 m thick sand layer. The speed of sound for water c was measured immediately before the experiments and amounted to 1510 m s^{-1} at a temperature of 8 °C. The acoustic signal source

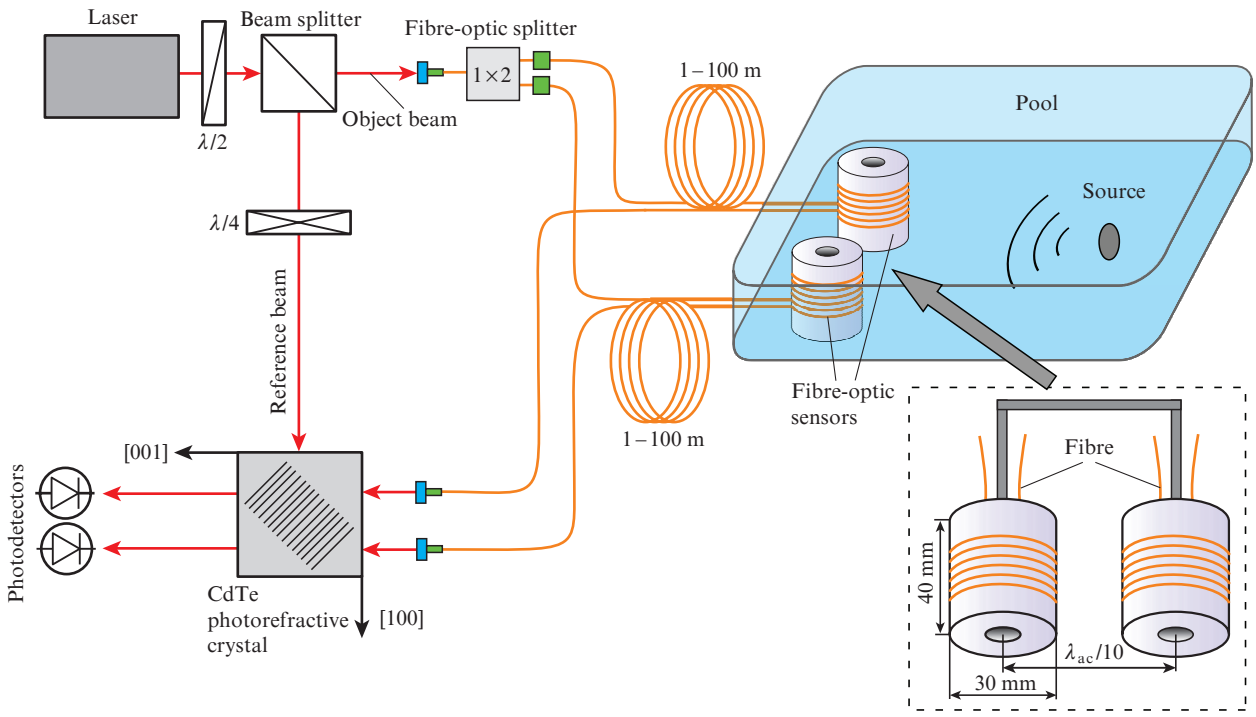

Figure 1. Scheme of a laser adaptive hydroacoustic intensimeter with the use of a fibre-optic sensing element.

was a Zetlab BC310 piezoelectric emitter. The emitter and receiver were located at the same depth (20 cm from the pool bottom).

In this work, the amplitude-frequency response of the laser intensimeter was experimentally measured (Fig. 2). For this purpose, a sinusoidal signal with a constant amplitude and variable frequency in the range of 1–100 kHz was applied to the emitter, while the fibre-optic sensors were located at a distance of $d = \lambda_{ac}/4$ from each other. As can be seen from Fig. 2, the intensimeter has a fairly uniform sensitivity in virtually the entire measured frequency range with a small resonance at a frequency of 8.1 kHz. At this frequency, the intensimeter sensitivity was 37 mrad Pa^{-1}. With this sensitivity, the developed intensimeter makes it possible to record weak signals with acoustic pressure starting from 3 mPa and intensity starting from 0.1×10^{-13} W m^{-2}.

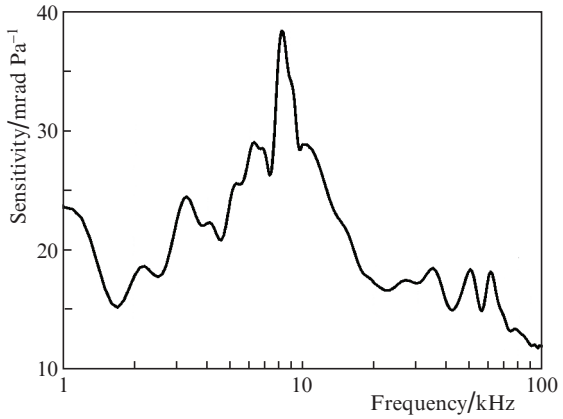

Figure 2. Amplitude–frequency response of the fibre-optic sensors of a hydroacoustic intensimeter.

Figure 3 shows an experimentally determined directional pattern of one of the sensors. As can be seen from this Figure, the sensor sensitivity is isotropic, which allows it to be successfully used in the intensimeter scheme.

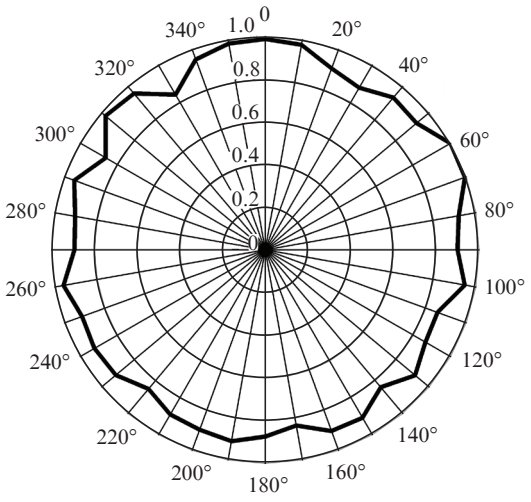

Figure 3. Directivity diagram of the fibre-optic sensor of a hydroacoustic intensimeter (solid bold curve is the normalised sensitivity measured in relative units).

Using the laser intensimeter developed, the acoustic field in the above-described pool was measured. The emitter was stationary, and the sensors were moved around the pool by means of a two-axis motorised translation stage providing positioning accuracy of ±1.5 mm in each direction (Fig. 4). The stage was controlled by a microcontroller using software developed in the Matlab environment, which also comprised recording and post-processing of the output signal from the intensimeter; this allowed automating the process of measuring the acoustic field parameters. During the measurement process, the intensimeter signals with duration of 0.25 s arriving via two channels were digitised at a sampling frequency of 96 kHz. The received signals were processed by an algorithm comprising the Fourier transform and the passage of a bandpass filter with a finite pulse response. Thus, the result of post-processing is a complex Fourier spectrum of the signal in the channel, containing the acoustic pressure values $p(\omega)$ at the measurement point, averaged over a time of 0.25 s. Experimental studies of the acoustic field were conducted at a frequency of 2.1 kHz, with an acoustic pressure of 0.2 Pa generated by the emitter in the near field determined using a calibrated piezoelectric sensor. A two-dimensional array of complex spectrum values was obtained as a result of measuring 130×65 points in the pool space with a step of 1 cm and further post-processing of the signal. Figure 5 shows the experimentally obtained acoustic complex pressure modulus (Fig. 5a) and its real part (Fig. 5c), displayed in the form of distribution maps over the measurement area.

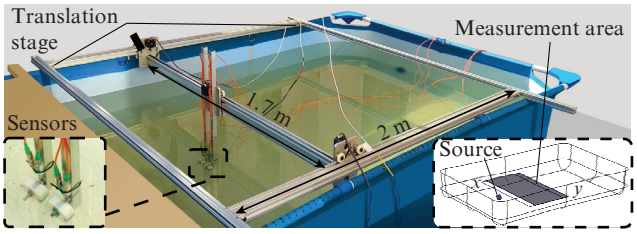

Figure 4. Test pool and motorised translation stage mounted on it.

To verify the measurement results, the acoustic field in the pool was simulated. The simulation was conducted in the ComsolMultiphysics software environment by solving a wave equation in a bounded domain with specified material parameters of water and environment. The computational domain geometry of the model makes allowance for the features of a real pool, such as rounding along the lower edges with a radius of 10 cm and the presence of a waist with a width of 5 cm. Figure 5 presents the results of simulating the modulus of the complex acoustic pressure (Fig. 5b) and its real part (Fig. 5d). It can be seen that the experimental results (Figs 5a and 5c) are in good agreement with the calculation results (Figs 5b and 5d). The inset in Fig. 4 shows the directions of the x and y axes. It should be noted that the emitter was located at a distance of 20 cm along the y axis from the beginning of the scanning region displayed in Fig. 5. Analysing the pressure modulus distribution, we can conclude that a stationary field is formed in the pool, which is very different from the field for free space. This means that the acoustic pressure modulus will not vary with the distance from the source quadratically, as in free space. The position of the pressure amplitude maxima depends on the acoustic signal

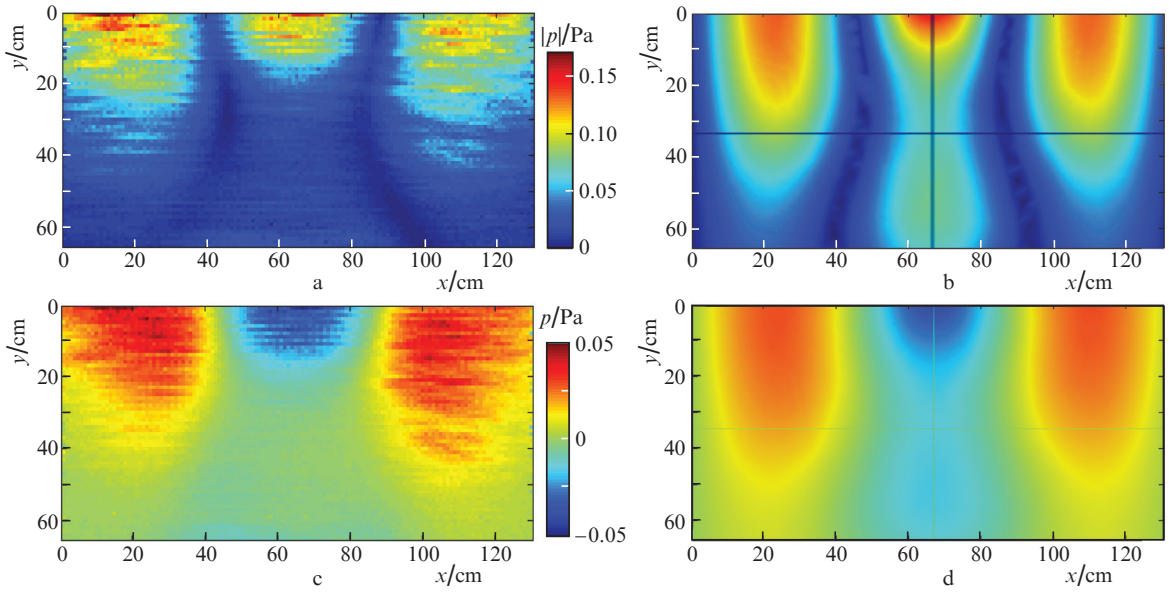

Figure 5. (Colour online) Results of measuring the acoustic field characteristics and their comparison with numerical calculation in a unified scale of values: (a) measured amplitude; (b) calculated amplitude field; (c) measured field (real part); (d) calculated field (real part).

frequency and the emitter location in the pool, and, accordingly, the intensity vector direction does not coincide with the direction to the emitter for each point in space. Therefore, to accurately determine the intensity vector direction inside the pool, we need to determine the x and y projections of the intensity vector. Using expression (1), we obtained the complex values of the gradient and pressure intensity for the x projection at the time moment of measurement at each point, since the sensitive elements are located in this projection. The additional y projection was calculated by substituting into (1) the measured values of the complex pressure from the previous rows and using an additional synchronising signal from the generator, which was recorded separately during the experiment. The results of calculating the x and y intensity projections (Figs 6a and 6c) are qualitatively consistent with the simulation data (Figs 6b and 6d), since the nature of their distributions in the measurement region is identical.

These two intensity projections are sufficient to construct a vector field in the plane (Fig. 7a), which is also consistent with the simulation results (Fig. 7b). It should be noted that the nature of the vector field distributions obtained both experimentally and numerically is in full agreement with the physics of acoustic wave propagation, which, in its propagation from the emitter, meets a wave reflected from the pool's flank and forms symmetrical regions with a swirl on the sides.

Thus, in this work, we have proposed a new type of laser fibre-optic vector-phase intensimeter based on a two-channel adaptive holographic interferometer and fibre-optic receivers

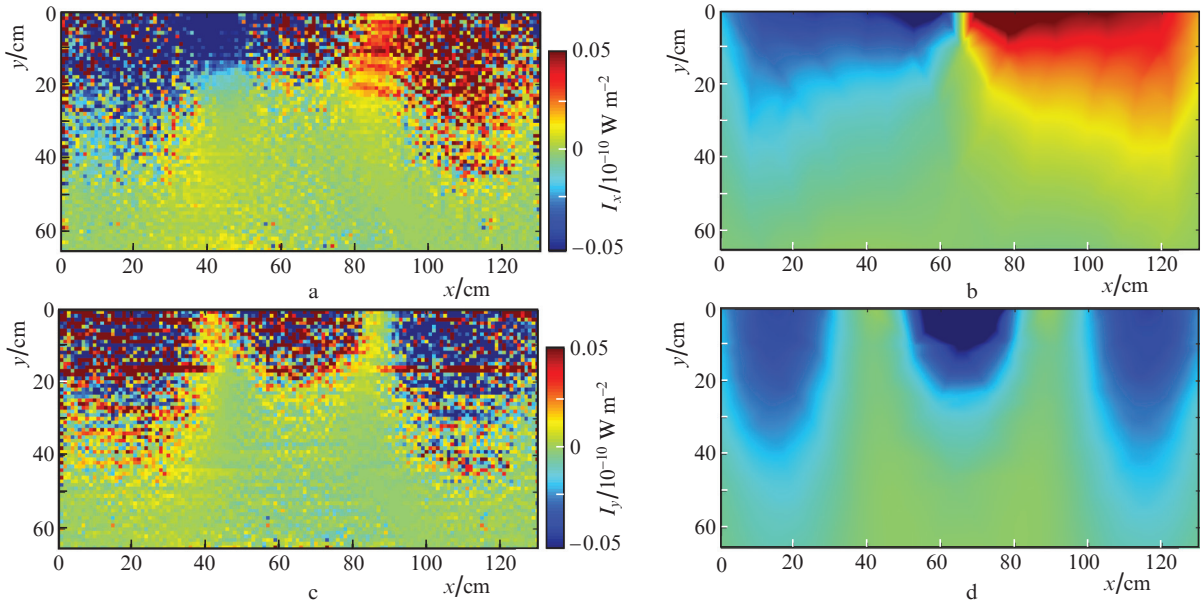

Figure 6. (Colour online) Intensity vector projections: (a) measured I_x; (b) calculated I_x; (c) measured I_y; (d) calculated I_y.

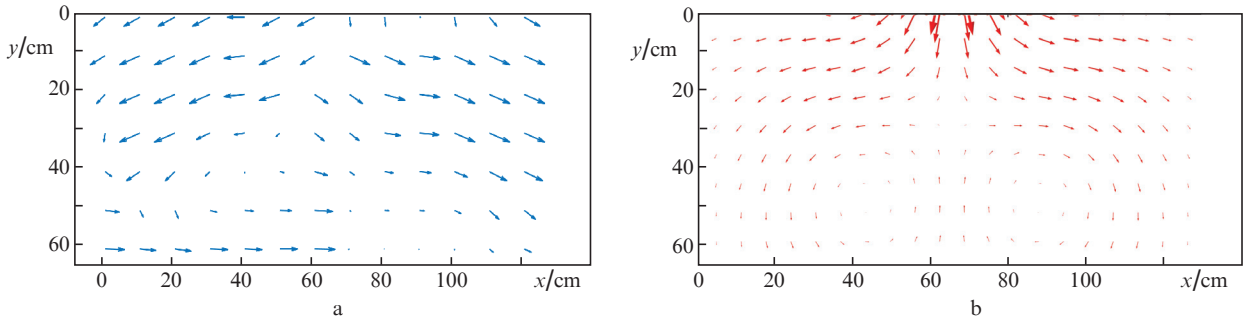

Figure 7. Reconstructed field of the acoustic intensity vector in the measurement region: (a) measured and (b) calculated.

of acoustic signals. The performance characteristics of the intensimeter were determined experimentally; the threshold sensitivity according to the acoustic field intensity amounted to 0.1×10^{-13} W m^{-2}. It is shown that the results of the experiment on measuring the intensity vector projection in a limited space are consistent with the results of numerical modelling. The use of measuring systems of this type makes it possible to record the intensity vector, as well as the energy, interphase, coherent, and probabilistic properties of ultra-weak acoustic fields, which facilitates the development of new effective detection algorithms and methods for determining the bearing of weak or significantly distant sources, as well as the development of methods for their classification.

Acknowledgements. This work was supported by the Russian Science Foundation (Grant No. 19-12-00323).

References

1. Sverdlin G.M. *Prikladnaya gidroakustika* (Applied hydroacoustics) (Leningrad: Sudostroyeniye, 1990).
2. Bjørnø L. *Applied Underwater Acoustics* (Amsterdam: Elsevier, 2017).
3. Busurin V.I., Nosov Yu.R. *Volokonno-opticheskiye datchiki* (Fibre-optic sensors) (Moscow: Energoatomizdat, 1990).
4. Udd E. *Fiber Optic Smart Structures* (New York: John Wiley & Sons, Inc., 1995).
5. Wagner J.W., Spicer J. *J. Opt. Soc. Am. B*, **4**, 1316 (1987).
6. Josten G., Lüthy W., Weber H.P. *Appl. Phys. B*, **51** (6), 418 (1990).
7. Karhade O., Degertekin L., Kurfess T. *Opt. Lett.*, **34** (19), 3044 (2009).
8. Kamshilin A.A., Petrov M.P. *Opt.Commun.*, **53**, 23 (1985).
9. Romashko R.V., Kulchin Y.N., Nippolainen E. *Laser Phys.*, **24** (11), 115604 (2014).
10. Romashko R.V., Bezruk M.N., Ermolaev S.A., Zavestovskaya I.N., Kulchin Y.N. *Bull. Lebedev Phys. Inst.*, **42** (7), 201 (2015).
11. Romashko R.V., Kulchin Yu.N., Bezruk M.N., Ermolaev S.A. *Quantum Electron.*, **46** (3), 277 (2016) [*Kvantovaya Elektron.*, **46** (3), 277 (2016)].
12. Kamenev O.T., Petrov Y.S., Hizhnyak R.V., Zavestovskaya I.N., Kulchin Y.N., Romashko R.V. *Bull. Lebedev Phys. Inst.*, **44** (7), 202 (2017).
13. Gordienko V.A. *Vektorno-fazovyye metody v akustike* (Vector-Phase Methods in Acoustics) (Moscow: Fizmatlit, 2007).
14. Gordienko V.A., Gordienko T.V., Krasnopistsev N.V., Nekrasov V.N. *Moscow Univ. Phys. Bull.*, **69**, 105 (2014) [*Vestn. Mosk. Univer. Ser. 3. Fiz., Astron.*, **2**, 3 (2014)].
15. Zakharov K.L. *Ustoych. Innov. Razv.: Proyekt. i Upravl.*, **10** (3), 148 (2014).
16. Romashko R.V., Bezruk M.N., Kamshilin A.A., Kulchin Yu.N. *Quantum Electron.*, **42** (6), 551 (2012) [*Kvantovaya Elektron.*, **42** (6), 551 (2012)].
17. Romashko R.V., Bezruk M.N., Ermolaev S.A., Storozhenko D.A., Kulchin Y.N. *Proc. SPIE*, **10176**, 1017612 (2017).
18. Dzyuba V.P. *Skalyarno-vektornyye metody teoreticheskoy akustiki* (Scalar-Vector Methods of Theoretical Acoustics) (Vladivostok: Dal'nauka, 2006).
19. Di Girolamo S., Kamshilin A.A., Romashko R.V., Kulchin Yu.N., Launay J.-C. *Opt. Express*, **15** (2), 545 (2007).
20. Romashko R.V., Di Girolamo S., Kulchin Y.N., Kamshilin A.A. *J. Opt. Soc. Am. B*, **27** (2), 311 (2010).
21. Bezruk M.N., Romashko R.V., Kulchin Yu.N., Ermolaev S.A., Notkin B.S. *Vestnik FEB RAS*, **2**, 117 (2019).